

EUROFEL-Report-2007-DS4-024

EUROPEAN FEL Design Study



Deliverable N°: D 4.13

Deliverable Title: SIMULATION AND TOLERANCE STUDIES ON THE
SELF-SEEDING OPTION AT FLASH

Task: DS-4

Author: V. Miltchev, J. Rossbach

Contract N°: 011935

**Project funded by the European Community
under the “Structuring the European Research Area” Specific Programme
Research Infrastructures action**

SIMULATION AND TOLERANCE STUDIES ON THE SELF-SEEDING OPTION AT FLASH*

V. Miltchev[†], J. Rossbach, Hamburg University, 22761 Hamburg, Germany

Abstract

In order to improve the temporal coherence of the radiation generated by the Free-electron LASer in Hamburg (FLASH), a two-stage seeding scheme is presently under construction [1]. It consists of two undulator stages separated by a magnetic chicane and a monochromator. In this report the performance of the self-seeded FEL is studied in simulations. An emphasis is placed on the tolerances of the most critical components and parameters.

INTRODUCTION

The basic setup of the self-seeding option [1, 2] is illustrated in Fig.1. It consists of two undulator stages separated by a magnetic chicane and a monochromator. The first (seeding) undulator operates as a conventional SASE FEL in the linear regime. After it, the electrons are separated from the SASE radiation. The electron beam passes

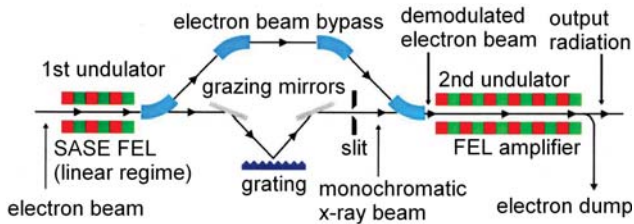


Figure 1: Schematic layout of the self-seeding setup.

through the magnetic bypass, that is used to remove the longitudinal charge density modulation (micro bunching). The radiation pulse is spectrally filtered in a high resolution grating monochromator [3] and afterwards is superimposed with the electron beam at the entrance of the second (seeded) undulator. Thus the monochromatic photon beam serves as a coherent radiation seed, which is amplified up to saturation in the second undulator. The concept of the self-seeding has the advantage that it is independent of any external radiation source and the seed is naturally synchronized with the electron bunch. An additional advantage is that the seeding wavelength is continuously tuneable. The monochromator optics, to be installed at FLASH, is designed for operation in the 6-60 nm range [2]. As shown in the example for 6 nm in Fig.2, the self-seeding increases the spectral brilliance by about two orders of magnitude, i.e. the output power of the seeded FEL is concentrated in a single line which is about a hundred times narrower than

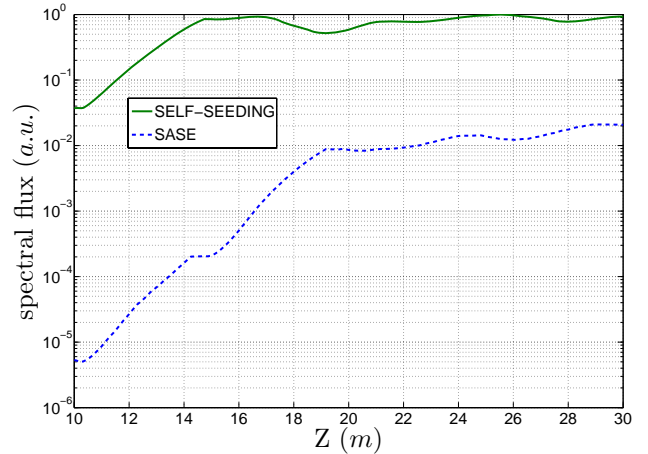


Figure 2: The spectral flux as a function the second (seeded) undulator length. Compared to the conventional SASE FEL, the self-seeding technique produces about two orders of magnitude higher spectral flux.

the spectrum of the conventional SASE FEL. It is important to note, that the gain in the first undulator section is essential for the effective operation of the self-seeded FEL. The output power level should be sufficiently low (about two-three orders of magnitude below saturation) in order to preserve the energy spread and the emittance of the electron beam. On the other hand the power of the seed, obtained from the first stage, should be much higher than the power of the shot noise in the second undulator.

ELECTRON OPTICS

Undulator stages

The undulator stages for the self-seeding option are subdivided into segments of about 4.5 m length. The first and the second undulator consist of three and six such segments respectively. A separated focusing system for the undulator stages is used at FLASH [5]. The focusing is accomplished by quadrupole doublets placed in-between two neighbouring undulator segments. The main feature of such focusing scheme, relevant to the implementation of the self-seeding, is the variable quadrupole strength. The total length of the first undulator (about 14.5 m) is optimized for operation at a wavelength in the order of 6 nm. The minimum average β -function for this case is about 4.5 m. As mentioned above, the power gain in the first undulator is crucial for the performance of the self-seeded FEL. Therefore, in order to compensate the scaling of the gain with the wavelength, one can vary the quadrupoles strength i.e. tune the average

* This work has been partially supported by the EU Commission in the Sixth Framework Program, Contract No. 011935-EUROFEL

[†] velizar.miltchev@desy.de

β -function accordingly.

Electron bypass

The bypass has to meet various requirements in order to ensure the proper operation of the self-seeding. The most essential of them are summarized in the following:

- Generation of an additional path length for the electrons, which is equal to the extra path length of the photons in the monochromator.
- Reduction of the micro bunching generated by the SASE process along the first undulator section.
- Adjustment of the electron optics to the undulator optics of for radiation wavelengths in the range 6-60 nm.
- Correction of the first and second order dispersion, minimization of the degradation of beam quality due to coherent synchrotron radiation effects.

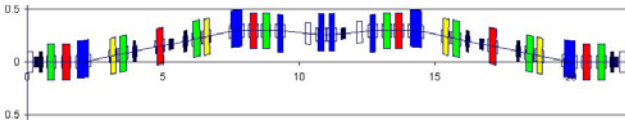


Figure 3: Final magnet layout of the electron bypass for the Seeding Option (side view). *black*: steerer, *blue*: dipole, *green*: quadrupole, vertical focusing, *red*: quadrupole, horizontal focusing, *yellow*: sextupole.

Therefore in contrast to the simplified scheme shown in Fig.1, the final design of the electron bypass optics [2] sketched in Fig.3, has a much more sophisticated layout.

SIMULATION TECHNIQUES

The simulation studies presented in this report divide into three groups:

- investigations on the performance of the self-seeded FEL
- estimation of the impact of the coherent synchrotron radiation (CSR)
- simulations to determine the tolerances of some critical parameters and components

The rest of this section gives a brief overview of the simulation tools and methods used for the studies listed above.

Performance of the self-seeded FEL

The performance of the self-seeded FEL has been studied with a modified version the 3-D time dependent FEL-code GENESIS [7]. The modification allows including the magnetic chicane by the means of a 6×6 transfer matrix and thus enables GENESIS to simulate consistently the complete self-seeding set-up. Following the general layout

of the self-seeding option, one splits the simulation into two parts. In the first part one examines the seeding undulator, which as mentioned before operates as a conventional SASE FEL. The complete particle distribution at the undulator exit is saved for later use in the next simulation step. In the second run, the previously obtained particle distribution is transformed with the help of the bypass matrix and then is tracked through the second undulator section. A certain wavelength λ_{seed} and average power P_{seed} is assumed for the external seed, which should be obtained at the output of the monochromator beamline. It is helpful to remind that the seed power should fulfil the requirement $P_{seed} \gg P_{shot}$, where P_{shot} is the effective shot noise power. Since $P_{shot} \leq 100$ W, $P_{seed} \approx 10$ kW has been assumed in all cases. The electron beam parameters, which have been assumed in the simulations, are summarized in Table 1

Table 1: Nominal electron beam parameters for operation at 6 nm

Energy, E_0	1000 MeV
Peak current, I_0	2500 A
rms energy spread	0.2 MeV
Normalized rms emittance, ϵ_n	2 mm mrad
rms bunch length, σ_z	50 μ m

Studies on CSR effects

These investigations follow a similar scheme as the one described above. However, in order to include the coherent synchrotron radiation in the numerical calculations, the bypass has been simulated together with the first undulator section with the ELEGANT [8] code. The program incorporates 1-D CSR algorithm [9] for dipoles and drift spaces. The produced particle distribution file is afterwards analyzed and converted into averaged slice information, which is used by GENESIS to simulate the interaction between the electrons and the radiation field along the second undulator section. In order to quantify the influence of the CSR effects, the described procedure has been repeated twice. Once including the CSR effects and second time with the CSR algorithm switched off. The average spectral flux has been considered as a figure of merit to compare the radiation quality for the two cases. As suggested in [4], in order to avoid numerical artefacts a large number of macro particles ($\sim 10^6$) was used in the ELEGANT simulations. The code ELEGANT has been used also for the calculations of the electron optics, to find the electron beam matching conditions and for the calculation of the transfer matrix of the bypass.

SELF-SEEDING PERFORMANCE

The first (seeding) undulator

As it is pointed out in [5], one of the main features of the separate focusing is the increased minimum aver-

age beta function $\langle\beta\rangle$. For the case of electron energy $E_0=1000\text{ MeV}$, corresponding to a wavelength $\lambda \approx 6\text{ nm}$, a minimum average β -function of about 4.5 m can be achieved. As shown in Fig.4, the design of the electron optics allows operation with the same $\langle\beta\rangle$ at the both sides of the magnetic chicane. For such setup the first stage works

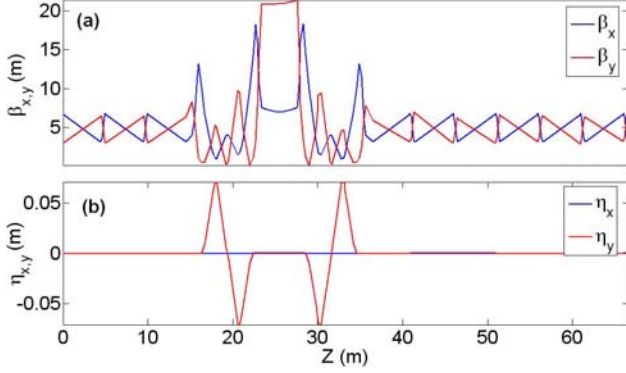


Figure 4: β -function (a) and dispersion (b) along the self-seeding electron beamline.

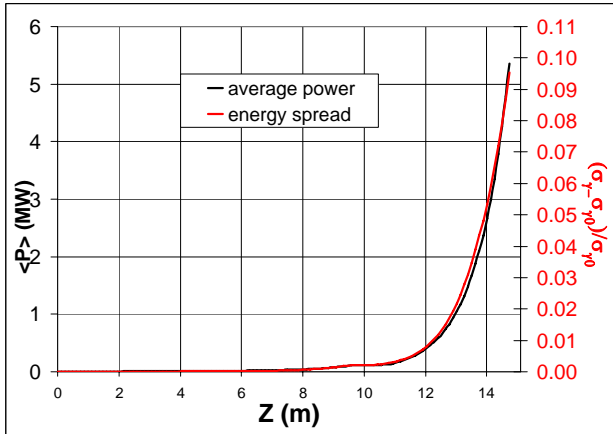


Figure 5: Average radiation power and fractional energy spread growth (right axis) along the first undulator.

in linear regime (see Fig.5) with an average power of the output radiation of about 5 MW. Again in Fig.5 the evolution of the energy spread growth along the undulator is shown. Essential there is the increase, which is induced by the FEL process. According to the simulation results, an energy spread increase in the order of 10% should be tolerable for the nominal electron beam parameters for operation at 6 nm (see Table 1 above). For operation at electron beam energy of 325 MeV (the lower design limit), corresponding to a resonant wavelength of about 60 nm, one has to consider modifications in the electron optics of the first undulator section and the chicane. These changes are necessary because of the scaling of the FEL gain with the wavelength. The electron optics designed for 6 nm, with $\langle\beta\rangle \approx 4.5\text{ m}$ (see Fig.4), provides saturation length in the order of 20 m for SASE mode. For the 60 nm case,

however, the saturation length is only about 9 m, which is significantly shorter than the first undulator (14.5 m) and therefore not acceptable from the point of view of the self-seeding option. One possible solution, as illustrated in Fig.6, is to increase $\langle\beta\rangle$ in the first stage to a value in the order of 25 m, corresponding to the desired linear SASE mode of operation (see Fig.7).

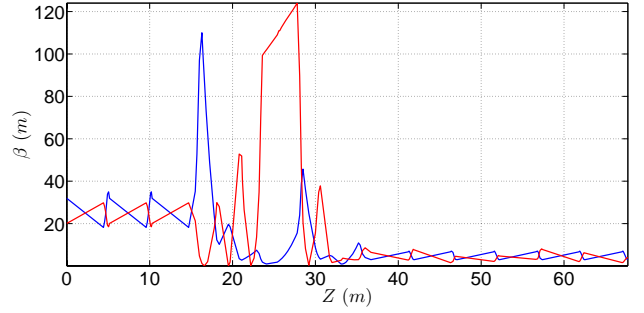


Figure 6: β -function along the self-seeding electron beamline using the modified optics in the first undulator section.

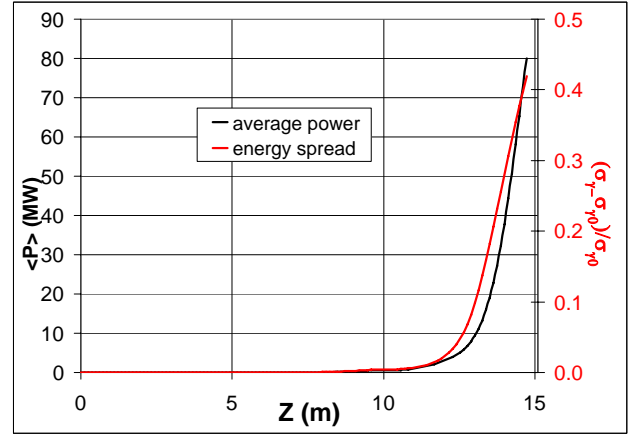


Figure 7: Average radiation power and fractional energy spread growth (right axis) along the first undulator with the modified $\langle\beta\rangle$ for 60 nm case.

The second (seeded) undulator

The proper operation of the electron bypass should ensure that the microbunching, induced in the first undulator, is removed so that at the beginning of the second undulator one starts with an unbunched electron beam. The micro bunching after the bypass is reduced by a factor of $\exp\left(-\frac{1}{2}\sigma_\delta^2 R_{56}^2 k_L^2\right)$ [6]. Here σ_δ is the fractional momentum spread, R_{56} is the momentum compaction factor of the bypass and $k_L = 2\pi/\lambda_L$ the radiation wavenumber. Figure 8 shows the radiation power and bunching as a function of the length of the second undulator. The simulation results demonstrate that the momentum compaction factor of the bypass $R_{56} \approx 0.73\text{ mm}$ is sufficient for the reduction of

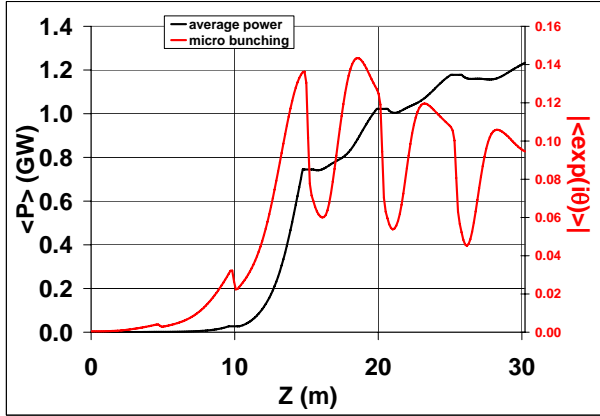


Figure 8: Radiation power and micro bunching (right axis) along the second undulator.

the micro bunching induced in the first undulator. A feature of the implemented separate focussing is the debunching taking place in the quadrupole doublets in-between the undulator segments [5]. It is mainly due to an introduced by the quadrupoles coupling between the transverse motion and the longitudinal position (resp. ponderomotive phase). Such coupling can be quantified with the help of the second order matrix elements T_{5ij} , $i, j = 1...4$. On the plot in Fig.8 the debunching appears as kinks at the locations of the quadrupole doublets e.g. at $Z \approx 5$ m, $Z \approx 10$ m etc. The

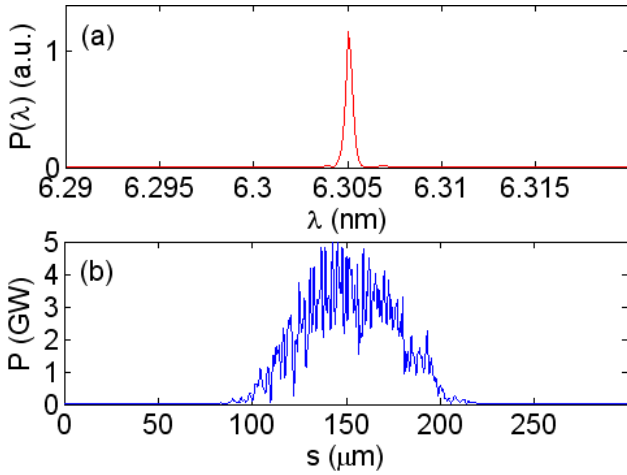


Figure 9: Spectrum (a) and power along the radiation pulse (b) in the second (seeded) section at the onset of the nonlinear regime ($Z \approx 15.5$ m).

simulation results plotted in Fig.9 demonstrate the effect of the self-seeding on the spectrum and the power of the output radiation. The two graphs in Fig.9 correspond to the onset of the nonlinear regime (see Fig.8). Further increase of the output power is coupled with a spectral broadening and in consequence with reduction of the spectral flux. As studied in [10], the length of the second undulator can be optimized in order to compensate the large fluctuations of

the seed intensity after the monochromator.

CSR effects

The electron bunches entering the magnetic chicane are of rms length $\sigma_z \approx 50 \mu\text{m}$ and high peak current $I_0 \approx 2.5$ kA. Therefore, despite the small bending angle $\theta = 3^\circ$,

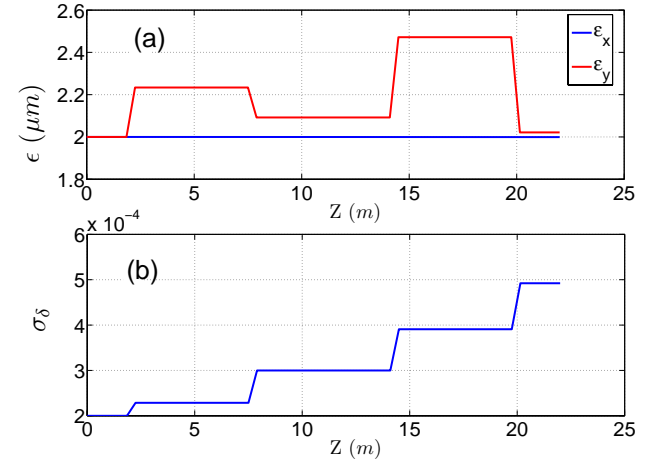


Figure 10: The normalized projected emittance (a) and the fractional momentum spread (b) along the magnetic chicane.

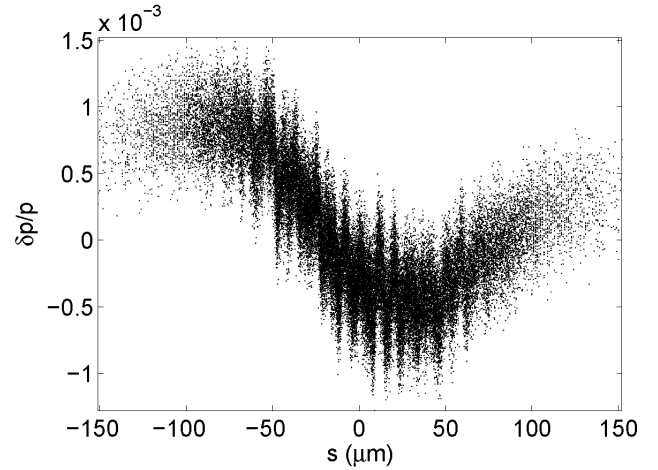


Figure 11: Distortion of the longitudinal phase space due to synchrotron radiation produced in the bypass dipoles.

the coherent component of synchrotron radiation generated in the bypass dipoles can be significant and might dilute the electron beam quality. The ELEGANT simulations, depicted in Fig.10, predict a projected emittance growth in the order of a percent. The slice emittance is, however, almost unchanged. For this reason the CSR effects on the transverse phase space can be considered as negligible. A much more significant impact on the longitudinal phase space is expected, as presented in Fig.11. The total relative energy spread has increased from 2×10^{-4} up to about 5×10^{-4} . The growth of the energy spread is due to the correlation

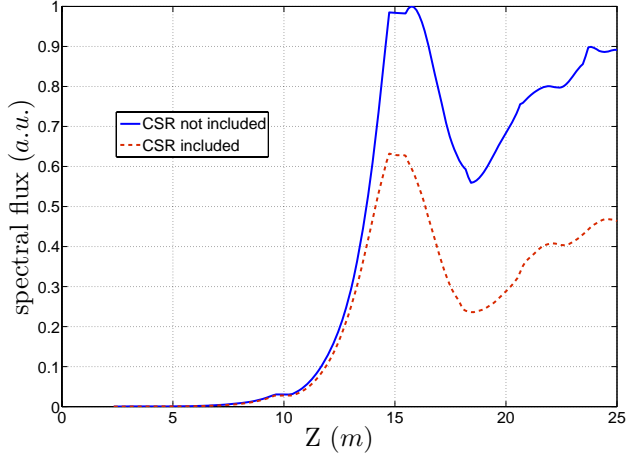


Figure 12: Demonstration of the impact of CSR effects - the spectral flux as a function of the undulator length.

in the longitudinal phase space created by the synchrotron radiation. The increased energy spread will drive more particles outside of the amplifier bandwidth and as a result one anticipates a reduction of the gain. Moreover the correlation in the phase space produces side bands in the spectrum or in other words spectral broadening. Fig.12 shows that there is about a factor of two decrease in spectral flux due to CSR effects. It is important to note that the worst case scenario has been considered i.e. the bypass optics and electron beam parameters have not been tuned to mitigate the impact of CSR.

TOLERANCE STUDIES

In the following, consideration is given to the influence of key electron beam properties and beamline components. Tolerances are specified for some critical parameters such as electron beam transverse offset and tilt, energy jitter, dispersion and its derivative, electron beam mismatch as well as quadrupoles displacement and gradient errors. Of interest is to see how simulations help to improve the design of an FEL.

Transverse offset and tilt of the electron beam

Whenever the electron bunch enters the 2nd undulator with an offset and(or) tilt it undergoes betatron oscillations as it propagates downstream. The excited coherent transverse motion disturbs the spatial overlap between the radiation field and the electron bunch. In addition it modulates the longitudinal velocity of the electrons and thus affects their ponderomotive phase with respect to the radiation field. These two effects, the so called beam wander and phase shake, result in FEL performance degradation. As pointed out in [12, 13] a betatron oscillation of amplitude smaller than the beam size degrades the FEL performance mainly by the poor transverse overlap while the phase shake becomes dominant for larger amplitudes. Fig-

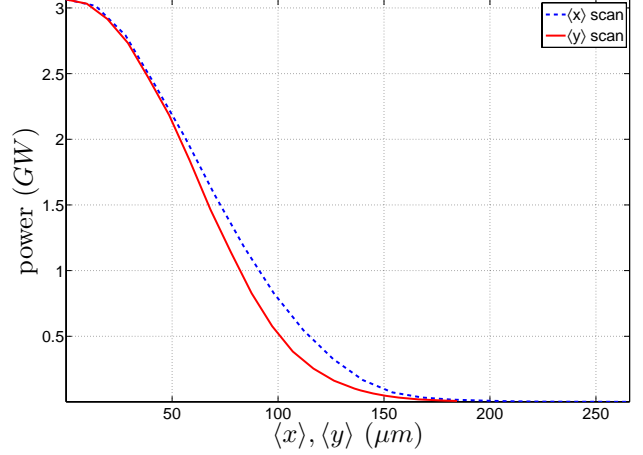


Figure 13: Radiation power vs. electron beam transverse offset $\langle x \rangle$ and $\langle y \rangle$ at the entrance of the 2nd undulator.

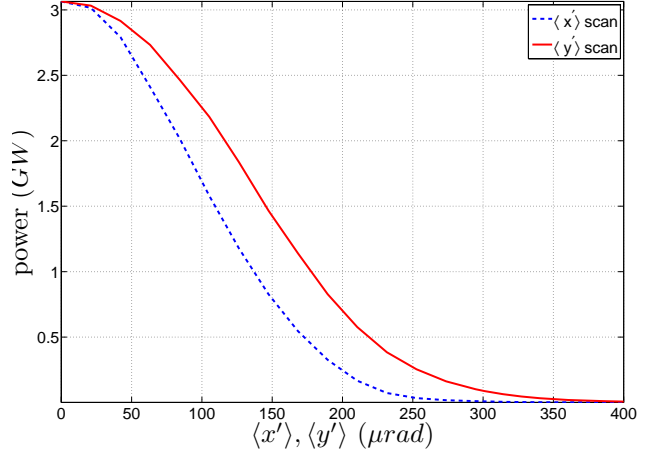


Figure 14: Radiation power vs. electron beam tilt $\langle x' \rangle$ and $\langle y' \rangle$ at the entrance of the 2nd undulator.

ure 13 shows the saturated power for electron beam of different transverse offsets at the beginning of the seeded undulator. With a radiation power tolerance $\Delta P/P_0$ of 10% (assumed as a guiding line here and in the rest of the tolerance studies) one obtains upper limits for the beam wander: $\Delta \langle x \rangle = \Delta \langle y \rangle \approx 20 (\mu m)$. These limits equal about 25% of the electron beam size $\sigma_x = \sigma_y \approx 70 (\mu m)$. The simulation results, depicted in Fig.14, show the saturation power as a function of the initial tilts $\langle x' \rangle$ and $\langle y' \rangle$. Considerations similar to the ones above yield the tolerances for the tilt in both transverse directions: $\Delta \langle x' \rangle \approx 4 (\mu rad)$ and $\Delta \langle y' \rangle \approx 6 (\mu rad)$. The pronounced difference between the horizontal and the vertical directions is due to the undulator focussing, which makes the tolerance in $\langle y' \rangle$ more relaxed.

Energy stability and dispersion

The operation of the self-seeding option has been simulated for various electron bunch energies. As shown in

Fig.15 the 10% radiation power tolerance is met for a relative energy deviation $\Delta\gamma/\gamma_0 < 3 \cdot 10^{-4}$, which complies with the experimental result of $2 \cdot 10^{-4}$ measured at FLASH. The obtained energy stability tolerance equals

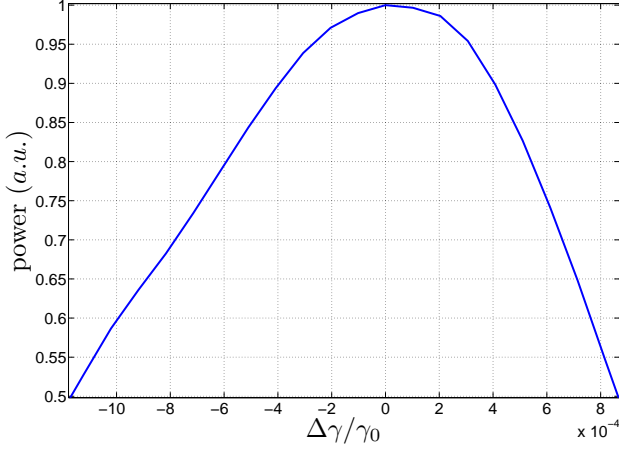


Figure 15: Radiation power vs. electron beam fractional energy deviation.

about 20% compared to $\rho_{3d} \approx 1.4 \cdot 10^{-3}$. Given the tolerable limits for the fractional energy deviation ($\Delta\gamma/\gamma_0 \approx 3 \cdot 10^{-4}$), beam transverse offset ($\Delta\langle x \rangle = \Delta\langle y \rangle \approx 20 (\mu\text{m})$) and angle ($\Delta\langle x' \rangle \approx 4 (\mu\text{rad})$ and $\Delta\langle y' \rangle \approx 6 (\mu\text{rad})$) one can specify tolerances for the dispersion and its derivative at the beginning of the seeded undulator:

$$\eta_x = \frac{\Delta\langle x \rangle}{\Delta\gamma/\gamma_0} = \eta_y \approx 67 (\text{mm}) \quad (1)$$

$$\eta'_x = \frac{\Delta\langle x' \rangle}{\Delta\gamma/\gamma_0} \approx 13 (\text{mrad}) \quad (2)$$

$$\eta'_y = \frac{\Delta\langle y' \rangle}{\Delta\gamma/\gamma_0} \approx 20 (\text{mrad}) \quad (3)$$

Offsets of bypass quadrupoles

This section addresses the accuracy of the transverse beam position control in the bypass (e.g. BPM resolution, corrector magnets strength etc.). Here, for convenience, one considers an offset of a quadrupole with respect to the beam orbit. The effect however will be the same if the beam propagates with an offset with respect to the quadrupole magnetic axis.

An offset Δx_q (Δy_q) of a quadrupole creates a dipole field proportional to the quadrupole gradient. If the misaligned quadrupole is located in the self-seeding bypass there are two major effects to be considered:

- Increased dispersion downstream. The dispersion at the beginning of the 2^{nd} undulator must remain within the limits specified in Eqs.(1-3)
- Electron beam steering due to the resulting dipole field. The beam transverse offset and tilt, at the beginning of the 2^{nd} undulator, must remain smaller than

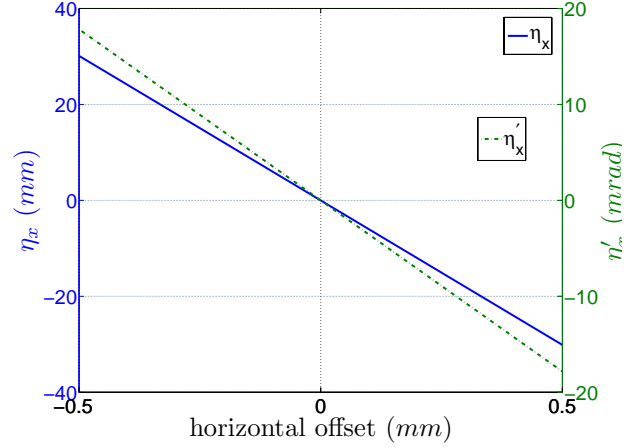


Figure 16: Horizontal dispersion η_x and its derivative η'_x at the beginning of the 2^{nd} undulator vs. the horizontal offset of one of the bypass quadrupoles.

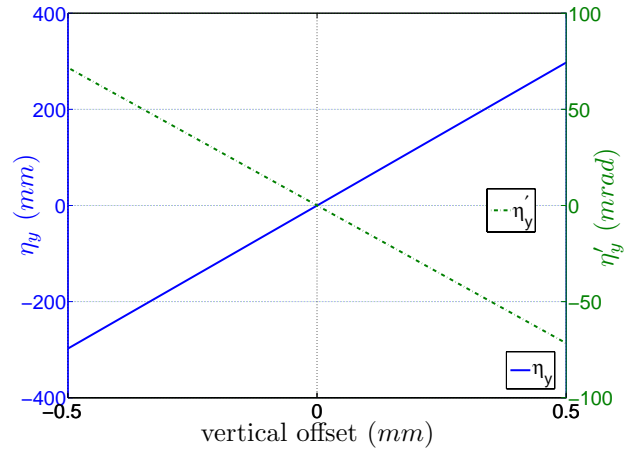


Figure 17: Vertical dispersion η_y and its derivative η'_y at the beginning of the 2^{nd} undulator vs. the vertical offset of one of the bypass quadrupoles.

the limits $\Delta\langle x \rangle$, $\Delta\langle y \rangle$, $\Delta\langle x' \rangle$ and $\Delta\langle y' \rangle$ discussed above.

The graphs in Fig.16 and Fig.17 depict the dependence of the dispersion and its derivative as a function of the quadrupole offset. Albeit all individual quadrupoles in the bypass have been studied, results are presented only for those, which have the strongest effect on the dispersion. If one considers only the increase of the dispersion and its derivative, the quadrupole offsets do not impose very tight tolerances. Provided that $\Delta x_q, \Delta y_q \leq 0.1 (\text{mm})$ is fulfilled, η and η' will remain in the range defined by Eqs.(1-3). A much more critical for the FEL performance is the effect of steering the electron beam due to the generated dipole field. By comparison between Figs.(18-19) and Figs.(13-14) one obtains tolerances in the micrometer range: $\Delta x_q, \Delta y_q < 3 (\mu\text{m})$ (as above $\Delta P/P_0 = 10\%$ is assumed). Again all quadrupoles in the bypass have

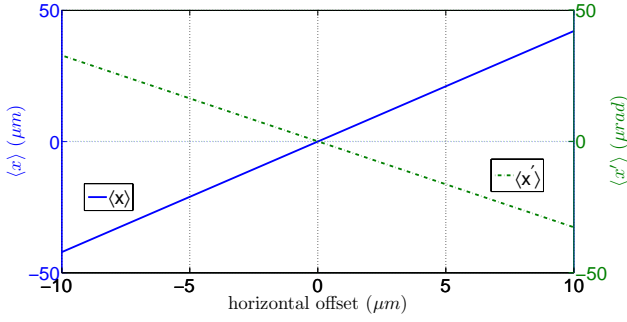


Figure 18: Transverse and angular beam offset, $\langle x \rangle$ and $\langle x' \rangle$, at the beginning of the 2nd undulator vs. the horizontal offset of one of the bypass quadrupoles.

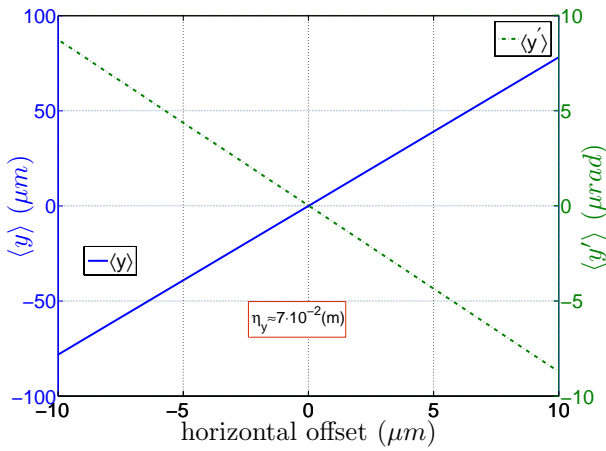


Figure 19: Transverse and angular beam offset, $\langle y \rangle$ and $\langle y' \rangle$, at the beginning of the 2nd undulator vs. the vertical offset of one of the bypass quadrupoles.

been studied individually, but results are presented only for those, producing the strongest steering effect.

The quadrupole investigated in Fig.19 has a peculiarity, which needs a separate discussion. This quadrupole is located at a position with a nonzero dispersion $\eta_y \approx 7 \text{ (cm)}$. Given the small allowed transverse jitter $\Delta \langle y \rangle < 3 \text{ (}\mu\text{m)}$ and $\eta_y \neq 0$, it is necessary to reconsider the energy stability requirements:

$$\Delta\gamma/\gamma_0 = \frac{\Delta \langle y \rangle}{\eta_y} < 5 \cdot 10^{-5} \quad (4)$$

One has to recall that the previous estimate $\Delta\gamma/\gamma_0 < 3 \cdot 10^{-4}$ (see Fig.15) has been obtained considering solely the operation of the seeded undulator. The new requirement $\Delta\gamma/\gamma_0 < 5 \cdot 10^{-5}$ follows from the investigations on the complete system "magnetic chicane+undulator". Clearly for further stabilization, one needs to implement a monitor for a feedback system, which should be able to measure the beam energy better than the desired energy stability of $5 \cdot 10^{-5}$ (see e.g. [14]). A complementary approach is to modify the bypass optics in order to have the quadrupoles at locations of zero (or sufficiently low) dispersion. Invest-

tigations on this option are ongoing. Taking into account Eq.(4), the dispersion defined in Eqs.(1-3) can be rescaled:

$$\eta_x = \frac{\Delta \langle x \rangle}{\Delta\gamma/\gamma_0} = \eta_y \approx 0.4 \text{ (m)} \quad (5)$$

$$\eta'_x = \frac{\Delta \langle x' \rangle}{\Delta\gamma/\gamma_0} \approx 80 \text{ (mrad)} \quad (6)$$

$$\eta'_y = \frac{\Delta \langle y' \rangle}{\Delta\gamma/\gamma_0} \approx 120 \text{ (mrad)} \quad (7)$$

Effect of a mismatched electron beam

In the simulations so far it was assumed the electron beam is perfectly matched to the undulator optics. In practice, due to e.g. quadrupole gradient errors in the chicane, the matching might not be ideal. This leads to larger betatron amplitude, hence higher longitudinal velocity spread and subsequently increased rms phase shake. As a result one anticipates FEL performance degradation. The lasing is also affected by the variation of the current density caused by the increased variation of the transverse beam size. In order to quantify the matching it is convenient to use the so called mismatch parameter ξ defined as [15]:

$$\xi = \frac{1}{2}(\beta\gamma_D - 2\alpha\alpha_D + \beta_D\gamma) \quad (8)$$

where α, β and γ are the Twiss parameters and the subscript D denotes the design values. For a matched beam $\xi = 1$ and for a mismatched beam $\xi > 1$. The results

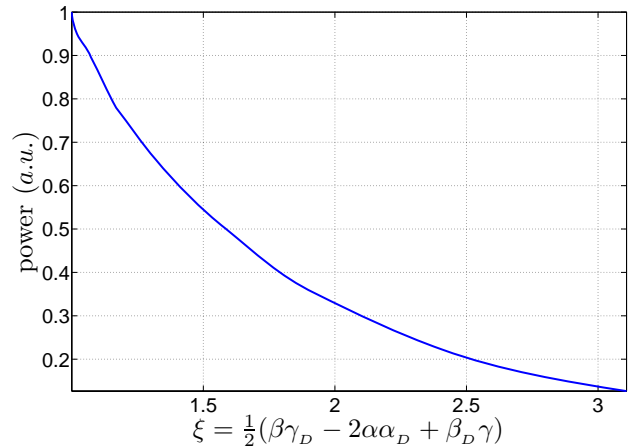


Figure 20: Radiation power vs. mismatch parameter in the horizontal plane at the beginning of the 2nd undulator.

of the GENESIS simulations plotted in Fig.20 and Fig.21 show the saturation power as a function of the mismatch parameter (evaluated at the beginning of the 2nd undulator). The 10% power tolerance sets the limits of the mismatch to:

$$\xi_x, \xi_y < 1.1 \quad (9)$$

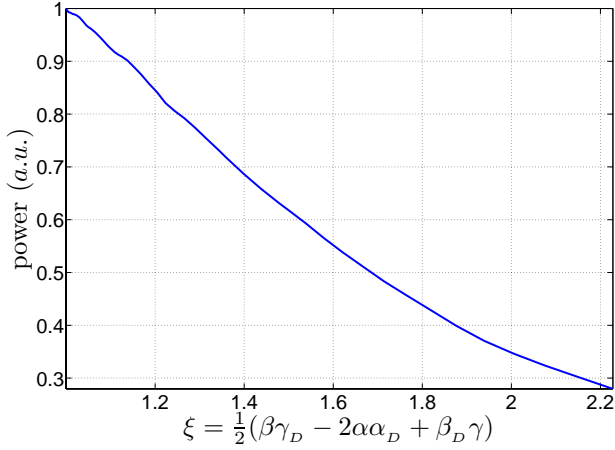


Figure 21: Radiation power vs. mismatch parameter in the vertical plane at the beginning of the 2nd undulator.

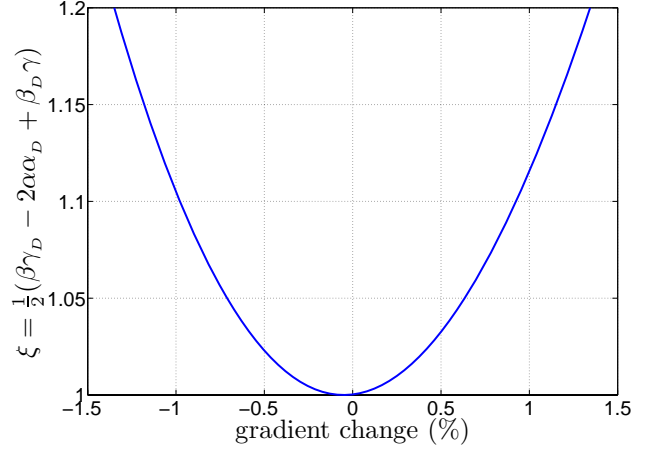


Figure 23: The mismatch parameter in the vertical plane vs. the relative gradient deviation of a bypass quadrupole.

Quadrupole gradient errors in the bypass

The gradient errors of the bypass quadrupoles are closely related to the previously discussed electron beam mismatch. When quadrupole errors are present, the electron beam will not be matched to the undulator optics and the FEL output power will be reduced. In such cases the mismatch parameter should remain in the limits defined in Eq.(9). The results of the investigations with ELEGANT,

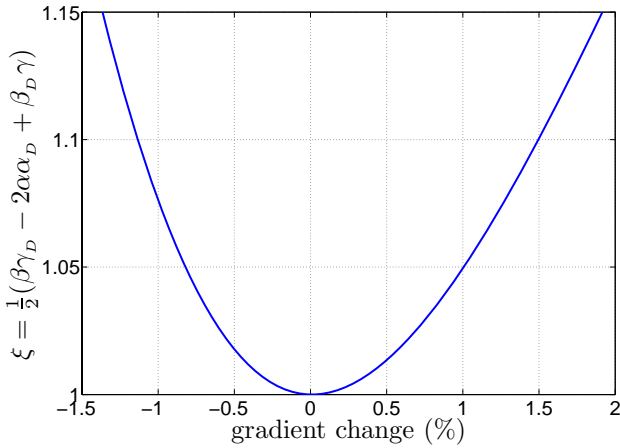


Figure 22: The mismatch parameter in the horizontal plane vs. the relative gradient deviation of a bypass quadrupole.

depicted in Fig.22 and Fig.23, show the typical variation of the mismatch parameter with the quadrupole gradient. Similar to before, although all quadrupoles in the bypass have been studied individually, results are shown only for the ones generating the largest mismatch. From the simulation results and taking into account Eq.(9) it follows the relative gradient error $\Delta g/g_0$ of the bypass quadrupoles should not exceed 1%.

CONCLUSIONS AND OUTLOOK

The operation of the two stage FEL has been studied, taking into account all the details in the design of the electron optics. The impact of the coherent synchrotron radiation emitted in the bypass dipoles was studied. The simulations predict about a factor of two reduction of the spectral flux due to CSR. Tolerances of critical parameters have been specified. Consideration was given to the influence of the electron beam tilt and offset, the energy stability, the effect of a mismatched electron beam, bypass quadrupole misalignment and gradient errors. The discussed requirements and tolerances are summarized as follows:

- maximal beam offset at the beginning 2nd undulator: $\Delta\langle x \rangle = \Delta\langle y \rangle < 20 (\mu m)$
- maximal beam tilt at the beginning 2nd undulator: $\Delta\langle x' \rangle < 4 (\mu rad)$, $\Delta\langle y' \rangle < 6 (\mu rad)$
- maximal dispersion at the beginning 2nd undulator: $\eta_x = \eta_y < 0.4 (m)$
- maximal dispersion derivative at the beginning 2nd undulator: $\eta'_x < 80 (mrad)$, $\eta'_y < 120 (mrad)$
- maximal energy jitter: $\Delta\gamma/\gamma_0 < 5 \cdot 10^{-5}$
- maximal offset of beam orbit with respect to a bypass quadrupole center: $\Delta x_q = \Delta y_q < 3 (\mu m)$
- required BPM resolution in the range of $\sim 1 (\mu m)$
- maximal quadrupole gradient error: $\Delta g/g_0 < 1 \%$
- maximal mismatch (see Eq.(8)): $\xi < 1.1$

Further studies including wave front propagation through the monochromator beamline are ongoing [11].

ACKNOWLEDGEMENTS

We thank Bart Faatz and Rolf Treusch for the many fruitful discussions and Atoosa Meseck for the modifications of the code GENESIS.

REFERENCES

- [1] J. Feldhaus et. al., *Opt. Commun.*, 140 (1997), 341
- [2] R. Treusch et. al. "The Seeding Project for the FEL in TTF Phase II", HASYLAB Annual Report 2001
- [3] R. Reisinger et. al., *Nucl. Instr. and Meth. A* (2001) 467-468, 38
- [4] M.A. Bowler et.al., "A study of CSR induced microbunching using numerical simulations", EPAC, 2004, Lucerne, Switzerland
- [5] B. Faatz et. al., *Nucl. Instr. and Meth. A* 475 (2001), 603
- [6] E.L. Saldin et al., *Nucl. Instr. and Meth. A* 539 (2001), 499
- [7] S. Reiche, *Nucl. Instr. and Meth. A* 429 (1999), 243
- [8] M. Borland, "elegant: A Flexible SDDS-Compliant Code for Accelerator Simulation," *Advanced Photon Source LS-287*, September 2000.
- [9] M. Borland, *Phys. Rev. ST Accel. Beams* 4, 070701 (2001)
- [10] E.L. Saldin et al., *Nucl. Instr. and Meth. A* 445 (2000), 178
- [11] Johannes Bahrndt et.al., "The Properties of the FEL Output for Self Seeding", FEL conference, 2006, Berlin, Germany
- [12] S. Reiche, *Nucl. Instr. and Meth. A* 445 (2000) 139
- [13] B. Faatz, J. Pflüger, Y.M. Nikitina, *Nucl. Phys. and Meth. A* 393 (1997) 380.
- [14] K. Hacker et. al., "Beam pickup designs suited for an optical sampling technique", FEL conference, 2006, Berlin, Germany
- [15] M. Minty and F. Zimmermann, "Measurements and control of charged particle beams", Springer, Berlin, Heidelberg, New York, 2003.